Title
Monocytes promote liver carcinogenesis in an oncogene-specific manner

Journal
Journal of Hepatology, 64(4)

ISSN
0168-8278

Authors
Juric, Vladislava
Ruffell, Brian
Evason, Kimberley J
et al.

Publication Date
2016-04-01

DOI
10.1016/j.jhep.2015.11.025

Peer reviewed

HHS Public Access

Author manuscript

J Hepatol. Author manuscript; available in PMC 2017 April 01.

Published in final edited form as:

J Hepatol. 2016 April ; 64(4): 881–890. doi:10.1016/j.jhep.2015.11.025.

Monocyte-dependent liver injury promotes carcinogenesis in an oncogene-specific manner

Vladislava Juric[1], **Brian Ruffell**[2], **Kimberley J. Evason**[3], **Junjie Hu**[4,5], **Li Che**[4,6], **Linlin Wang**[3], **Xin Chen**[4,5], and **J. Michael Bishop**[1]

[1]GW Hooper Research Foundation, University of California, San Francisco, San Francisco, CA 94143, USA

[2]Department of Immunology, H. Lee Moffitt Cancer Center & Research Institute, Tampa, FL 33612, USA

[3]Department of Pathology, University of California, San Francisco, San Francisco, CA 94143, USA

[4]Department of Bioengineering and Therapeutic Sciences, University of California, San Francisco, San Francisco, CA 94143, USA

[5]School of Pharmacy, Hubei University of Chinese Medicine, Wuhan, Hubei, P.R. China

[6]Key laboratory of Carcinogenesis and Translational Research (Ministry of Education), Peking University Cancer Hospital and Institute, Beijing, P. R. China

Abstract

Background & Aims—The leukocyte composition of tumors is heterogeneous, as is the involvement of each leukocyte subset in promoting or restraining tumorigenesis. This heterogeneity reflects the tissue of origin, tumor stage, and the functional state of leukocyte activation, but its biological roots remain poorly understood. Since tumorigenesis is driven by various genetic events, we assessed the role of driver genes in shaping the profiles and the roles of leukocytes in tumorigenesis.

Methods—Mouse liver tumors were induced by hepatic overexpression of either *MYC* or the combination of myristoylated *AKT* and $NRAS^{V12}$ oncogenes via hydrodynamic transfection. A comparative, flow cytometry- and histology-based immunophenotyping of liver-infiltrating leukocytes was performed at various stages of liver tumorigenesis. The roles of the most abundant

Corresponding author: Vladislava Juric, Present address: Gilead Sciences, Foster City, CA 94404, USA, Phone: (650) 235-3360, vladi.juric@gilead.com.

Conflict of interest: The corresponding author V. Juric is currently an employee of Gilead Sciences. No potential conflicts of interest were disclosed by the other authors.

Author contributions: V.J. designed the study, acquired, analyzed and interpreted data, and prepared the manuscript; B.R. designed select experiments and analyzed data; K.E. and L.W. provided histopathological reviewing; X.C., L.C., and J.H. performed select experiments; V.J., B.R., and J.M.B. contributed to writing the manuscript.

leukocyte subsets in tumorigenesis were addressed by immunodepletion. The contribution of liver injury was assessed by comparing the injury-inducing hydrodynamic transfection model to a model in which *MYC* is an inducible transgene.

Results—Myristoylated *AKT* and *NRAS*^{V12} promoted a marked recruitment of CD11b^{+}Ly6G^{hi}Ly6C^{int} neutrophils and CD11b^{+}Ly6G^{-}Ly6C^{hi} monocytes to the liver, but their immunodepletion did not alter tumorigenesis. In contrast, despite minimal invasion by monocytes/neutrophils during *MYC*-driven tumorigenesis, immunodepletion of these cells reduced *MYC* tumor burden and extended survival. *MYC*-driven tumor-initiation was augmented specifically by Ly6C^{+} monocytes and their ability to promote liver injury.

Conclusions—Our results demonstrate that leukocyte profiles do not necessarily predict their involvement in tumorigenesis, that the functional role of leukocytes can be shaped by oncogenes, and that monocyte-dependent tissue injury selectively cooperates with *MYC* during tumorigenesis.

Keywords

oncogenes; *MYC*; *AKT*; *RAS*; tumor; inflammation; neutrophils; monocytes; liver injury

Introduction

While acquisition of driver genetic lesions is necessary to initiate and maintain tumors [1], the influence of tumor stroma on tumor development is now also widely appreciated [2, 3]. Tumor-infiltrating leukocytes play dual roles in cancer, with the potential to either restrain or facilitate tumorigenesis. Most solid tumors are infiltrated by leukocytes with diverse profiles [4], possibly reflecting the tissue of origin and tumor stage [5-7]. However, the precise role of driver genes in mediating leukocyte infiltration and function has been largely unexplored. Understanding the biological roots of this heterogeneity is important, because leukocyte subtype density and location within tumors can serve as a predictor of clinical outcomes and response to therapy [8].

Oncogenes can activate tumor cell-intrinsic transcriptional programs that elicit production of inflammatory mediators and promote myeloid cell recruitment [9-13]. For example, in the early stages of pancreatic β-cell carcinogenesis driven by *MYC* and *BCL-X*$_{L}$ co-expression, interleukin-1β-triggered angiogenesis is sustained by infiltrating mast cells [10, 13]. Similarly, mutant *Kras*-expression by pancreatic ductal epithelial cells sustains tumor growth by mediating myeloid cell recruitment and fostering an immunosuppressive microenvironment [11, 12]. However, these studies do not address the role of particular oncogenes in shaping of these immunological features, which may relate at least partially to the tissue and/or cell type being examined. For example, ibrutinib – purportedly through blockade of mast cell activation – suppresses growth of mutant *Kras*-driven pancreatic ductal adenocarcinoma [14].

It is also unclear the degree to which oncogene-driven inflammation interplays with extrinsic inflammation. Extrinsic inflammation caused by tissue injury or infection increases cancer risk and can be indispensable for tumorigenesis in some cases [5, 15, 16]. The link between inflammation and cancer is particularly evident in liver cancer [17], which typically

develops in the setting of chronic viral hepatitis and cirrhosis of various etiologies [18]. These risk factors promote liver damage, and the liver regeneration response – thought to be mediated by inflammatory cells secreting soluble inflammatory mediators – drives compensatory hepatocyte proliferation and promotes tumorigenesis [19, 20].

To study oncogene-specific regulation of immune responses in liver tumors, we utilized mouse models for liver cancer driven by overexpression of *MYC* or the combination of myristoylated *AKT1* (*myrAKT)* and $NRAS^{V12}$ oncogenes (*AKT/RAS*) [21, 22]. These models are amenable for comparative analysis, since both rely on the same method of hydrodynamic transfection of oncogenes and produce tumors in the same tissue type, with similar latency. Moreover, *MYC*, *AKT*, and *RAS* oncogenes have been implicated in human liver cancers. *MYC* is overexpressed in up to 70% of viral and alcohol-related human hepatocellular carcinomas (HCC) [23], the serine-threonine kinase AKT is activated in 23% of human HCCs [24], and the RAF/MEK/ERK pathway – which can be triggered by *RAS* – is activated in all human HCCs [25].

We performed a comparative, flow cytometry-based immunophenotyping of liver-infiltrating leukocytes at various stages of liver tumorigenesis driven by *MYC* and *AKT/RAS*, assessed the roles of the most abundant myeloid subsets by immunodepletion, and addressed the contribution of tissue injury to tumorigenesis.

Materials and methods

Animals and hydrodynamic transfection

Hydrodynamic injection [26] was performed on 6-8 weeks old female FVB mice from Jackson Laboratory (Bar Harbor, ME). Injections contained 1 μg of plasmid DNA/0.1 ml saline/gr mouse. pT3-EF1 α-***MYC*** [22], or the combination of pT3-EF1 α-*myrAKT1*-HA and pT-CAGGS-$NRAS^{V12}$ [21] plasmid ratio to Sleeping Beauty transposase (pCMV-SB) [21] was 25:1 (w/w). The transgenic Tet-o-MYC/LAP-tTA (LT2-MYC) mice were described previously [27]. All animal studies conformed to National Institutes of Health guidelines and were approved by University of California Institutional Animal Care and Use Committee.

Flow cytometry

Livers were perfused with phosphate-buffered heparin, minced, and incubated in phosphate-buffered saline (PBS) containing 1 mg/ml Collagenase A (Roche) and 50 units/ml DNase I (Roche) for 30 min at 37°C. Digestion was quenched by adding FACS buffer (1 mM EDTA and 2% FBS in PBS) and single-cell suspensions were obtained by filtering through 70 μm cell strainers (BD Biosciences). Erythrocytes were removed by 5 min incubation in Pharm Lyse buffer (BD Biosciences). After washing in FACS buffer, $<10^6$ cells were incubated for 30 min on ice with rat anti-mouse CD16/CD32 mAb (Fc Block, BD Biosciences) diluted in PBS containing Live Dead Aqua (1:500, Life Technologies). Cells were then incubated in a mixture of fluorophore-conjugated mAbs (**Supplementary Table 2**) and fixed. Data was collected with LSR II (BD Biosciences) flow cytometer and analyzed using FlowJo software. Leukocytes were profiled based on the cell surface marker expression

(**Supplementary Table 1**). The number of each leukocyte subset/mm^2 tissue was calculated by combining the flow cytometry data (% of total CD45$^+$ cells) with CD45 IHC staining index (# of CD45$^+$ cells/mm^2 tissue).

Immunohistochemistry, automated image acquisition, and analysis

Perfused livers were formalin-fixed, and paraffin-embedded. Liver tissue sections (5 μm thick) were stained with hematoxylin and eosin (H&E). For antigen retrieval, sections were microwaved for 10 min in 0.01 M Na-citrate buffer (pH 6.0) and endogenous peroxidase was blocked with 3% H_2O_2. Primary antibodies (rat monoclonal anti-CD45 (clone 30-F11), BD Pharmingen; rabbit monoclonal anti-MYC (clone Y69), Abcam; biotinlylated rat monoclonal anti-neutrophil (clone 7/4), Cedarlane) were applied for 2 h in blocking buffer (2.5% BSA, 5% normal goat serum in PBS), followed by species-appropriate secondary antibodies (Vectastain ABC kit) and DAB reagents (Vector Laboratories). Hematoxylin or methyl green was used for counterstaining. Images were acquired with Axiophot microscope (Zeiss) equipped with Leica DFC 420 C digital camera and Leica FireCam software (Leica Microsystems). Whole-slide digital images of CD45 immunostaining were captured with the Aperio ScanScope XT Slide Scanner (Aperio Technologies). Digital images were analyzed using Aperio ImageScope software.

Immunoblot

Livers were homogenized in the lysis buffer containing 50 mM HEPES-KOH pH 7.4, 130 mM NaCl, 1% Triton X-100, 1% SDS, 1% sodium deoxycholate, and complete protease inhibitor cocktail (Roche). Lysates were boiled for 5 min in Laemmli buffer (50 mM Tris-HCl pH 6.8, 12.5% glycerol, 2% SDS, 0.01% bromophenol blue, and 100 mM DTT), and proteins were electrophoresed and immunoblotted. Blots were probed with anti-MYC (clone Y69, Abcam) and anti-GAPDH (clone 6C5, EMD Millipore), followed by HRP-conjugated secondary antibodies and ECL reagent (Amersham).

Protein array and ELISA

Livers were lysed in PBS containing 1% Triton X-100 and complete protease inhibitor cocktail (Roche). The lysates (150 μg/sample) were used in Proteome Profiler Mouse Cytokine Array (R&D Systems) or in CCL2 and CXCL1 Quantikine ELISA (R&D Systems).

In vivo leukocyte depletion

Mice were injected intraperitoneally (I.P.) with 200 μl of antibodies (BioXCell) in saline solution. Gr-1 mAb or control rat IgG2b (clone LTF-2) were injected every three days for the total of four treatments at 250 μg/mouse; 500 μg/mouse of anti-Ly6G mAb (clone 1A8) or control rat IgG2a (clone 2A3) was injected triweekly for total of 9 treatments; 200 μg/mouse of anti-CD11b mAb (clone M1/70) or control rat IgG2b (clone LTF-2) was injected at triweekly for total of 7 treatments. Anti-CSF-1 mAb (clone 5A1) or control IgG1 (clone HRPN) were given once, in a single dose of 1 mg Ab/mouse.

Serum ALT measurement

Whole-blood samples were allowed to coagulate for 15 min at room temperature and centrifuged at 1,000 *g* at 4°C for 10 min to separate the serum. Aminotransferase levels were measured using Automated Diagnostic Analyzer (IDEXX Laboratories).

Statistical analyses

Data were analyzed using the Student's *t*-test to compare between two groups. Two-way ANOVA was used to compare among several groups, followed by the Tukey's post-hoc test ($p = 0.05$) for pairwise comparison.

Results

Inflammation during liver tumorigenesis induced by *MYC* and *AKT/RAS*

To address how oncogenes shape the leukocyte responses in the liver during tumorigenesis, we induced liver tumors by hydrodynamic transfection of mice with *MYC* or *AKT/RAS* [21, 22]. Hepatic overexpression of *MYC* results in highly aggressive, poorly differentiated liver tumors that resemble human hepatoblastomas [22, 27]. Overexpression of constitutively active *myrAKT1* produces HCC with long latency [28], while $NRAS^{G12V}$ does not give rise to liver tumors because of *RAS*-induced senescence that clears pre-malignant hepatocytes [29]. Nevertheless, *NRAS* synergizes with oncogenic *AKT* to produce tumors that resemble moderately differentiated HCC and cholangiocarcinoma [21].

Hydrodynamic tail-vein injection confirmed earlier reports of transient liver injury [30, 31] that healed by 6 days post-injection (dpi), while hydrodynamic transfection of *MYC* or *AKT/RAS* caused progressive neoplastic changes (**Fig. 1A and Supplementary Fig. 1A-C**). Hepatic steatosis was prominent in *AKT/RAS* livers, in line with previous reports of *AKT*-driven lipogenesis [28]. *MYC* and *AKT/RAS* tumors developed with similar latency, reaching terminal stages ~7 weeks post-transfection. Immunodetection of CD45 in the liver (**Fig. 1A**) revealed that oncogenes promoted a transient inflammation in the form of large leukocyte clusters at the early stages of tumorigenesis (3 dpi). This was more pronounced in *AKT/RAS*- than in *MYC*-transfected livers, and was minimal in saline-injected livers. Despite leukocyte clusters in both models, only *AKT/RAS* triggered a marked increase in leukocyte infiltration over saline control at 3 dpi (**Fig. 1B**). However, the leukocyte density returned to baseline by 14 dpi and was relatively constant throughout tumor progression in both models (**Fig. 1B**). Expression of oncogenes was detected as early as 3 dpi (**Supplementary Fig. 1D**), confirming efficient oncogene delivery and suggesting that early inflammation could be linked to oncogene activation.

Distinct profiles of liver-infiltrating leukocytes during *MYC*- and *AKT/RAS*-driven tumorigenesis

To further characterize intrahepatic $CD45^+$ leukocytes, single-cell suspensions from the perfused livers were stained with antibodies against various leukocyte lineage markers (**Supplementary Table 1**) and analyzed by polychromatic flow cytometry. The assay revealed dynamic changes in the leukocyte composition over the course or tumorigenesis (**Fig. 2 and Supplementary Fig. 2A**). Hydrodynamic injection of saline promoted a

transient increase in macrophages, classical and plasmacytoid dendritic cells at 3 dpi, followed by the recruitment of $CD4^+$ T cells, B cells, and γδ T cells at the later stages (**Fig. 2**). While oncogene-transfected livers shared certain trends with controls, including macrophage recruitment, several oncogene-specific changes were observed. Specifically, *MYC*-expressing livers failed to recruit $CD4^+$ T lymphocytes, and terminal *MYC* tumors contained more NK cells than *AKT/RAS* tumors or the time-matched controls. *MYC* tumors also displayed a slight, yet significant increase in $Ly6C^+$ monocyte recruitment at 3 dpi compared to untreated mice ($p < 0.01$).

AKT/RAS promoted a marked recruitment of several myeloid cell populations into the livers at the early stages after transfection (3 dpi), including classical dendritic cells ($CD11c^{hi}MHCII^+$), neutrophils ($CD11b^+Ly6G^+Ly6C^{int}$), and monocytes ($CD11b^+Ly6G^-Ly6C^{hi}$) (**Fig. 2**). Although the effect was partially transient, all three of these populations were also increased at end-stage (49 dpi). $Ly6G^+$ neutrophils represented the dominant immune population throughout *AKT/RAS*-driven tumorigenesis (**Fig. 2 and Supplementary Fig. 2A**), and were particularly prominent in *AKT/RAS* compared to *MYC* tumors **(Fig. 3A)**. Transcript levels of monocyte/macrophage-derived cytokines, such as IL-6 and IL-1β, but not of TNFα, were higher in *AKT/RAS*- livers compared to *MYC*-transfected livers (**Supplementary Fig. 2B**). Immunostaining for 7/4 antigen, a differentiation marker associated specifically with neutrophils and monocytes [32], also corroborated that neutrophils and monocytes were more abundant in *AKT/RAS* livers (**Fig. 3B**).

To understand the difference in myeloid cell infiltration in the two models, we compared cytokine/chemokine expression in *AKT/RAS* and *MYC* tumors. A protein array identified several differentially expressed factors (**Fig. 3C**), including CCL2, a monocyte chemoattactant [33], and CXCL1, a neutrophil chemoattractant [34]. ELISA confirmed a transient induction of these chemokines by both oncogenes at the early stages of tumorigenesis (**Fig. 3D**) coinciding with inflammation (**Fig. 1B**). CXCL1 was 5-fold higher and CCL2 was 3-fold higher in *AKT/RAS*-compared to *MYC*-transfected livers, in line with a massive recruitment of neutrophils and monocytes specifically into *AKT/RAS* livers.

Gr-1^+ myeloid cells selectively augment *MYC*-driven tumorigenesis

We postulated that neutrophils and monocytes, abundant in *AKT/RAS*-expressing livers, might regulate tumorigenesis in this model, especially given that *Kras*-driven pancreatic ductal adenocarcinoma has previously been linked with GM-CSF production and recruitment of immunosuppressive Gr-1^+ (Ly6G/Ly6C) cells [11, 12]. Thus, we treated mice systemically with the anti-Gr-1 monoclonal antibody (mAb) RB6-8C5 to deplete leukocytes expressing Ly6G and/or Ly6C [35]. Flow cytometry analysis confirmed depletion of $Ly6G^+Ly6C^{int}$ neutrophils and $Ly6G^-Ly6C^{hi}$ monocytes, but not $Ly6G^-Ly6C^-MHCII^+F4/80^+$ macrophages, from the livers of both *MYC* and *AKT/RAS* mice (**Supplementary Fig. 3A**). We observed no reduction in dendritic cells or lymphocyte populations by anti-Gr-1 treatment (data not shown).

Since the leukocyte depletion by anti-Gr-1 was transient (**Supplementary Fig. 3B and C**), we began Gr-1 treatments at −1, +4, and +16 days relative to hydrodynamic transfection to examine the role of Gr-1$^+$ cells at different stages of tumorigenesis (**Supplementary Fig. 3D**). Unexpectedly, none of the treatment regimens altered the survival of *AKT/RAS* mice (**Fig. 4A**). In contrast, anti-Gr-1 mAb extended the survival of *MYC* mice when applied during the early stages of tumorigenesis (1 day before, or 4 days after hydrodynamic transfection) (**Fig. 4B**). No effect on survival was observed when Gr-1-depletion was performed at a later stage (16 dpi). Consistent with its effect on survival, anti-Gr-1 mAb reduced the burden of *MYC* tumors, but not that of *AKT/RAS* tumors, as determined by liver-to-body mass ratio (**Fig. 4C and D**). Additionally, the livers of anti-Gr-1-treated mice at 7 dpi contained fewer MYC-positive basophilic foci (**Fig. 4E**), suggesting that Gr-1$^+$ cells cooperate with *MYC* during tumor initiation rather than progression. This decrease in the number of MYC-positive foci was not due to impaired transfection efficiency, since we saw no reduction in GFP transfection by anti-Gr-1 mAb treatment (**Supplementary Fig. 4**).

Thus, despite the dramatic infiltration of neutrophils and monocytes resulting from *AKT/RAS* transfection, these cells apparently played no role in early tumorigenesis. Instead, even though invasion into the tissue was minimal following *MYC* transfection, neutrophils and/or monocytes cooperated with *MYC* to enhance tumorigenesis in the liver.

Ly6C$^+$ monocytes cooperate with MYC during tumorigenesis

We confirmed the selective involvement of myeloid cells in *MYC*-driven tumorigenesis through depletion of cells expressing CD11b (**Fig. 5A and B**). Surprisingly however, when we selectively depleted neutrophils using anti-Ly6G mAb (clone 1A8) (**Supplementary Fig. 5A**), we did not observe extended survival of *MYC* mice, or reduce tumor burden in either model (**Fig. 5C and D**), indicating that neutrophils were dispensable for tumorigenesis.

During liver damage, recruited CD11b$^+$Ly6C^{hi} monocytes can differentiate into pro-inflammatory and pro-fibrogenic macrophages [36]. Tumor-associated macrophages have also been shown to derive from Ly6C^{hi} monocytes [37]. We thus pre-treated mice with an anti-CSF-1 mAb to deprive macrophages of an important survival/recruitment factor [38-40], and significantly reduced the number of Ly6C$^-$F4/80$^+$MHCII$^+$ macrophages in the livers at 3 dpi (**Supplementary Fig. 5B**). However, the treatment did not alter the survival *MYC* or *AKT/RAS* mice, suggesting that macrophages do not regulate early stages of tumorigenesis in either model (**Fig. 5E and F**). By excluding the role of neutrophils and macrophages (**Fig. 5G**), the results suggest that Ly6C$^+$ inflammatory monocytes were the CD11b$^+$Gr-1$^+$ myeloid population responsible for augmenting tumorigenesis induced by *MYC*.

The role of tissue injury in monocyte-*MYC* cooperation

Ly6C$^+$ monocytes can promote tumor growth by suppressing tumor-specific T lymphocytes [41]. However, systemic depletion of CD8$^+$ T lymphocytes did not reverse the effect of anti-Gr1 mAb on survival of *MYC* mice (**Supplementary Fig. 7A and B**), indicating the involvement of an alternative mechanism. As anti-Gr-1 mAb extended survival only when

administered in the early stages of *MYC*-induced tumorigenesis, we hypothesized that the liver injury induced by hydrodynamic transfection might relate to the role of monocytes in promoting tumor development. We thus turned to the LT2-MYC transgenic mouse model, allowing for doxycycline-regulated, hepatocyte-specific expression of *MYC* transgene [27]. LT2-MYC liver tumors are histologically similar to those induced by hydrodynamic transfection of *MYC* [22, 42]. The onset of hepatic MYC expression in LT2-MYC mice occurred ~20 days after doxycycline removal (**Fig. 6A and B**) and the MYC-positive foci (**Fig. 6A**) progressed into tumors, replacing most of the normal liver by day 60.

To assess the role of Gr-1$^+$ leukocytes in the early stages of tumorigenesis in LT2-MYC mice, we began anti-Gr-1 mAb treatment 18 days after doxycycline removal, and found no effect on survival (log-rank test p=0.6) (**Fig. 6C**). It has been demonstrated that hydrodynamic injection shortens the LT2-MYC tumor latency, likely due to the injury-triggered liver regeneration [43]. Indeed, hydrodynamic injection of LT2-MYC mice with saline (HDI) accelerated tumor progression, although this was not statistically significant (log-rank test p=0.07). Critically, we found that anti-Gr-1 mAb treatment partially reversed the effect of hydrodynamic injection and extended survival (log-rank test p=0.01) (**Fig. 6C**). Thus, Gr-1$^+$ cells promoted *MYC*-driven tumorigenesis specifically in the context of liver injury.

Hydrodynamic injection promotes liver damage [44], and as expected, serum alanine transaminase (ALT) levels increased in the control-transfected mice at 3 dpi (**Fig. 6D**). *AKT/RAS* and *MYC* elicited a similar degree of liver injury, albeit higher than the control transfection (**Fig. 6D**), and also promoted hepatic apoptosis more so than the control (**Supplementary Fig. 6**). Anti-Gr1 mAb treatment reduced serum ALT levels by approximately 50% in the control- and oncogene-transfected groups (**Fig. 6D**). Liver damage, however, was neutrophil-independent, since anti-Ly6G mAb did not prevent the increase in serum ALT in any case (**Fig. 6D**). Together, these data demonstrate that *AKT/RAS* and *MYC* trigger a similar level of Ly6C$^+$ monocyte-dependent liver injury, but that monocytes only augment tumorigenesis driven by *MYC*.

Discussion

Most solid tumors are infiltrated by diverse leukocytes whose type, density, and location within tumors can serve as a prognostic factor [8]. Here we report the changes in tissue-infiltrating leukocyte profiles during tumorigenesis driven by distinct oncogenes in a single tissue type. Activation of *MYC* or co-activation of *AKT* and *RAS* in the livers of mice promoted a varying degree of inflammation and infiltration of distinct leukocyte subsets, thereby demonstrating that the leukocyte composition of a tissue is shaped, at least in part, by tumor-driving genetic lesions. Our finding that Ly6C$^+$ monocytes augment tumorigenesis driven by *MYC* was unexpected, considering the minimal hepatic infiltration of monocytes in this model. This suggests that the abundance of a given leukocyte subset in a pre-neoplastic tissue does not necessarily predict their role in tumorigenesis, and that their role is influenced by the type of tumor-initiating genetic lesion.

Myeloid cells, specifically neutrophils and monocytes, were markedly increased in the livers of *AKT/RAS*-transfected compared to *MYC*-transfected mice. Several oncoproteins, including MYC [10], RAS [9], RET [46] and EGFR [47] can activate tumor cell-intrinsic signaling pathways that drive production of pro-inflammatory cytokines and chemokines [5]. Loss of tumor suppressors p53, APC, or PTEN has also been implicated in regulation of tumor-associated inflammation [48, 49]. Here, we report that *AKR/RAS* co-activation in hepatocytes promotes an increase in CCL2 and CXCL1, and a massive recruitment of myeloid cells into the liver.

Recent work has demonstrated the functional significance of recruited Gr-1$^+$ leukocytes for liver tumorigenesis at the early stages of oncogenic $NRAS^{G12V}$ activation in hepatocytes [29]. In this model recruited Gr-1$^+$ monocytes act in cooperation with CD4$^+$ T lymphocytes to eliminate the *RAS*-expressing, pre-malignant senescent cells to restrain tumorigenesis [29]. Although we saw a similar massive recruitment of Ly6G$^+$ and Ly6C$^+$ leukocytes upon hepatic co-activation of *AKT* and *RAS*, we found that these cells were inconsequential for tumorigenesis. One possible explanation for why Ly6C$^+$ monocytes were irrelevant during *AKT/RAS* tumor development is the suppression of *RAS*-driven senescence by *AKT* [50]. Indeed, previous studies have not detected senescence in the *AKT/RAS* model [21], thus potentially eliminating the role for Ly6C$^+$ monocyte activity in senescence surveillance and tumorigenesis. Also, *AKT/RAS* signaling may confer hepatocytes with a superior proliferative capacity, allowing independence from the growth-promoting stimuli of the immune microenvironment. *AKT*-induced hepatic steatosis in *AKT/RAS* livers [28] may also drive hepatocyte proliferation independently of inflammation through oxidative stress-mediated JNK activation [51]. Thus, tumor-driving oncogenes are a critical determinant not only of the recruitment of myeloid cells to tissues, but also of their functional role.

While we found that monocytes play a role at the early stages of *MYC*-driven tumorigenesis, the precise timing of monocyte involvement and the molecular underpinnings of our observations remain unclear. Tumor-infiltrating myeloid cells promote tumorigenesis via multiple mechanisms [52, 53]. For example, they can sustain tumor cell survival and proliferation through secretion of pro-inflammatory cytokines [54], promote angiogenesis [55], blunt cytotoxic T cell activity by fostering an immunosuppressive microenvironment [11, 12], or prevent senescence [49]. Although we did not find a role for CD8$^+$ T cells, future studies will be necessary to understand the mechanisms by which monocytes specifically enhance *MYC*-driven tumorigenesis.

The common causes of liver cancers in humans, including viral hepatitis, cirrhosis, alcoholic and toxin injury, promote liver damage and inflammation [56]. Comparing the injury-inducing hydrodynamic injection model to an inducible *MYC* overexpressing transgenic model, we found that *MYC*-driven tumor-initiation was augmented specifically by Ly6C$^+$ monocytes recruited to the liver during injury. Since we found that both *MYC* and *AKT/RAS* promote similar levels of monocyte-dependent liver injury, it remains to be addressed why injury and/or monocytes selectively enhance *MYC*-driven tumor initiation. *MYC* tumors are poorly differentiated and resemble human hepatoblastomas, whereas *AKT/RAS* tumors resemble moderately differentiated HCC and cholangiocarcinoma [21, 22, 27]. These histological distinctions may make these two models inherently different in their

susceptibility to immune regulation. Intriguingly, *MYC* is clinically associated with the injury-induced viral and alcohol-related HCC, but not with cryptogenic HCC [23], and *MYC* expression increases with hepatic injury in a chemically-induced liver cancer model [57]. These clinical observations correlate with our finding that *MYC*-driven liver tumorigenesis is injury dependent, and indicate that additional studies on the interplay between *MYC*-driven tumorigenesis, liver injury and monocytes are warranted.

Supplementary Material

Refer to Web version on PubMed Central for supplementary material.

Acknowledgements

We thank members of the Bishop laboratory for critical feedback; L.M. Coussens (Oregon Health and Science University, Portland, OR) for valuable discussion of preliminary results; L. Urisman and K. Jusewicz-Haidle (University of California, San Francisco, San Francisco, CA) for assistance with animal husbandry; and the UCSF Parnassus Flow Cytometry shared core resource, supported by Diabetes Research Center Grant (NIH P30 DK063720).

Financial support: This work was supported by UCSF/G.W. Hooper Research Foundation Endowment Funds and by NIH R01CA136606 grant from the National Institutes of Health to XC.

Abbreviations

myrAKT	myristoylated *AKT1*
AKT/RAS	*myrAKT* and *NRAS*
HCC	hepatocellular carcinoma
PBS	phosphate-buffered saline
H&E	hematoxylin and eosin
I.P.	intraperitoneal
dpi	days post-injection
mAb	monoclonal antibody

References

1. Pagliarini R, Shao W, Sellers WR. Oncogene addiction: pathways of therapeutic response, resistance, and road maps toward a cure. EMBO Rep. 2015
2. Quail DF, Joyce JA. Microenvironmental regulation of tumor progression and metastasis. Nat Med. 2013; 19:1423–1437. [PubMed: 24202395]
3. Hanahan D, Coussens LM. Accessories to the crime: functions of cells recruited to the tumor microenvironment. Cancer Cell. 2012; 21:309–322. [PubMed: 22439926]
4. Tlsty TD, Coussens LM. Tumor stroma and regulation of cancer development. Annu Rev Pathol. 2006; 1:119–150. [PubMed: 18039110]
5. Mantovani A, Allavena P, Sica A, Balkwill F. Cancer-related inflammation. Nature. 2008; 454:436–444. [PubMed: 18650914]
6. Ruffell B, Au A, Rugo HS, Esserman LJ, Hwang ES, Coussens LM. Leukocyte composition of human breast cancer. Proc Natl Acad Sci U S A. 2012; 109:2796–2801. [PubMed: 21825174]

7. Coussens LM, Zitvogel L, Palucka AK. Neutralizing tumor-promoting chronic inflammation: a magic bullet? Science. 2013; 339:286–291. [PubMed: 23329041]
8. Fridman WH, Pagès F, Sautès-Fridman C, Galon J. The immune contexture in human tumours: impact on clinical outcome. Nat Rev Cancer. 2012; 12:298–306. [PubMed: 22419253]
9. Sparmann A, Bar-Sagi D. Ras-induced interleukin-8 expression plays a critical role in tumor growth and angiogenesis. Cancer Cell. 2004; 6:447–458. [PubMed: 15542429]
10. Shchors K, Shchors E, Rostker F, Lawlor ER, Brown-Swigart L, Evan GI. The Myc-dependent angiogenic switch in tumors is mediated by interleukin 1beta. Genes Dev. 2006; 20:2527–2538. [PubMed: 16980582]
11. Bayne LJ, Beatty GL, Jhala N, Clark CE, Rhim AD, Stanger BZ, et al. Tumor-derived granulocyte-macrophage colony-stimulating factor regulates myeloid inflammation and T cell immunity in pancreatic cancer. Cancer Cell. 2012; 21:822–835. [PubMed: 22698406]
12. Pylayeva-Gupta Y, Lee KE, Hajdu CH, Miller G, Bar-Sagi D. Oncogenic Kras-induced GM-CSF production promotes the development of pancreatic neoplasia. Cancer Cell. 2012; 21:836–847. [PubMed: 22698407]
13. Soucek L, Lawlor ER, Soto D, Shchors K, Swigart LB, Evan GI. Mast cells are required for angiogenesis and macroscopic expansion of Myc-induced pancreatic islet tumors. Nat Med. 2007; 13:1211–1218. [PubMed: 17906636]
14. Masso-Valles D, Jauset T, Serrano E, Sodir NM, Pedersen K, Affara NI, et al. Ibrutinib exerts potent antifibrotic and antitumor activities in mouse models of pancreatic adenocarcinoma. Cancer Res. 2015; 75:1675–1681. [PubMed: 25878147]
15. Guerra C, Schuhmacher AJ, Canamero M, Grippo PJ, Verdaguer L, Perez-Gallego L, et al. Chronic pancreatitis is essential for induction of pancreatic ductal adenocarcinoma by K-Ras oncogenes in adult mice. Cancer Cell. 2007; 11:291–302. [PubMed: 17349585]
16. de Martel C, Franceschi S. Infections and cancer: established associations and new hypotheses. Crit Rev Oncol Hematol. 2009; 70:183–194. [PubMed: 18805702]
17. Pikarsky E, Porat RM, Stein I, Abramovitch R, Amit S, Kasem S, et al. NF-[kappa]B functions as a tumour promoter in inflammation-associated cancer. Nature. 2004; 431:461–466. [PubMed: 15329734]
18. El-Serag HB. Epidemiology of Viral Hepatitis and Hepatocellular Carcinoma. Gastroenterology. 2012; 142:1264–1273. e1261. [PubMed: 22537432]
19. Maeda S, Kamata H, Luo JL, Leffert H, Karin M. IKKbeta couples hepatocyte death to cytokine-driven compensatory proliferation that promotes chemical hepatocarcinogenesis. Cell. 2005; 121:977–990. [PubMed: 15989949]
20. Sakurai T, Maeda S, Chang L, Karin M. Loss of hepatic NF-kappa B activity enhances chemical hepatocarcinogenesis through sustained c-Jun N-terminal kinase 1 activation. Proc Natl Acad Sci U S A. 2006; 103:10544–10551. [PubMed: 16807293]
21. Ho C, Wang C, Mattu S, Destefanis G, Ladu S, Delogu S, et al. AKT and N-Ras co-activation in the mouse liver promotes rapid carcinogenesis via mTORC1, FOXM1/SKP2, and c-Myc pathways. Hepatology (Baltimore, Md). 2012; 55:833–845.
22. Tward AD, Jones KD, Yant S, Kay MA, Wang R, Bishop JM. Genomic progression in mouse models for liver tumors. Cold Spring Harb Symp Quant Biol. 2005; 70:217–224. [PubMed: 16869757]
23. Schlaeger C, Longerich T, Schiller C, Bewerunge P, Mehrabi A, Toedt G, et al. Etiology-dependent molecular mechanisms in human hepatocarcinogenesis. Hepatology. 2008; 47:511–520. [PubMed: 18161050]
24. Boyault S, Rickman DS, de Reyniès A, Balabaud C, Rebouissou S, Jeannot E, et al. Transcriptome classification of HCC is related to gene alterations and to new therapeutic targets. Hepatology. 2007; 45:42–52. [PubMed: 17187432]
25. Hwang YH, Choi JY, Kim S, Chung ES, Kim T, Koh SS, et al. Over-expression of c-raf-1 proto-oncogene in liver cirrhosis and hepatocellular carcinoma. Hepatology Research. 2004; 29:113–121. [PubMed: 15163433]

26. Bell JB, Podetz-Pedersen KM, Aronovich EL, Belur LR, McIvor RS, Hackett PB. Preferential delivery of the Sleeping Beauty transposon system to livers of mice by hydrodynamic injection. Nature protocols. 2007; 2:3153–3165. [PubMed: 18079715]
27. Shachaf CM, Kopelman AM, Arvanitis C, Karlsson A, Beer S, Mandl S, et al. MYC inactivation uncovers pluripotent differentiation and tumour dormancy in hepatocellular cancer. Nature. 2004; 431:1112–1117. [PubMed: 15475948]
28. Calvisi DF, Wang C, Ho C, Ladu S, Lee SA, Mattu S, et al. Increased lipogenesis, induced by AKT-mTORC1-RPS6 signaling, promotes development of human hepatocellular carcinoma. Gastroenterology. 2011; 140:1071–1083. [PubMed: 21147110]
29. Kang TW, Yevsa T, Woller N, Hoenicke L, Wuestefeld T, Dauch D, et al. Senescence surveillance of pre-malignant hepatocytes limits liver cancer development. Nature. 2011; 479:547–551. [PubMed: 22080947]
30. Suda T, Gao X, Stolz DB, Liu D. Structural impact of hydrodynamic injection on mouse liver. Gene Ther. 2006; 14:129–137. [PubMed: 16988719]
31. Woodard LE, Hillman RT, Keravala A, Lee S, Calos MP. Effect of nuclear localization and hydrodynamic delivery-induced cell division on [phi]C31 integrase activity. Gene Ther. 2009; 17:217–226. [PubMed: 19847205]
32. Hirsch S, Gordon S. Polymorphic expression of a neutrophil differentiation antigen revealed by monoclonal antibody 7/4. Immunogenetics. 1983; 18:229–239. [PubMed: 6618532]
33. Tsou CL, Peters W, Si Y, Slaymaker S, Aslanian AM, Weisberg SP, et al. Critical roles for CCR2 and MCP-3 in monocyte mobilization from bone marrow and recruitment to inflammatory sites. J Clin Invest. 2007; 117:902–909. [PubMed: 17364026]
34. De Filippo K, Dudeck A, Hasenberg M, Nye E, van Rooijen N, Hartmann K, et al. Mast cell and macrophage chemokines CXCL1/CXCL2 control the early stage of neutrophil recruitment during tissue inflammation. Blood. 2013; 121:4930–4937. [PubMed: 23645836]
35. Fleming TJ, Fleming ML, Malek TR. Selective expression of Ly-6G on myeloid lineage cells in mouse bone marrow. RB6-8C5 mAb to granulocyte-differentiation antigen (Gr-1) detects members of the Ly-6 family. J Immunol. 1993; 151:2399–2408. [PubMed: 8360469]
36. Karlmark KR, Weiskirchen R, Zimmermann HW, Gassler N, Ginhoux F, Weber C, et al. Hepatic recruitment of the inflammatory Gr1+ monocyte subset upon liver injury promotes hepatic fibrosis. Hepatology. 2009; 50:261–274. [PubMed: 19554540]
37. Movahedi K, Laoui D, Gysemans C, Baeten M, Stange G, Van den Bossche J, et al. Different tumor microenvironments contain functionally distinct subsets of macrophages derived from Ly6C(high) monocytes. Cancer Res. 2010; 70:5728–5739. [PubMed: 20570887]
38. Ries CH, Cannarile MA, Hoves S, Benz J, Wartha K, Runza V, et al. Targeting tumor-associated macrophages with anti-CSF-1R antibody reveals a strategy for cancer therapy. Cancer Cell. 2014; 25:846–859. [PubMed: 24898549]
39. Ruffell B, Coussens LM. Macrophages and Therapeutic Resistance in Cancer. Cancer Cell. 2015; 27:462–472. [PubMed: 25858805]
40. Ruffell B, Chang-Strachan D, Chan V, Rosenbusch A, Ho CM, Pryer N, et al. Macrophage IL-10 blocks CD8+ T cell-dependent responses to chemotherapy by suppressing IL-12 expression in intratumoral dendritic cells. Cancer Cell. 2014; 26:623–637. [PubMed: 25446896]
41. Gallina G, Dolcetti L, Serafini P, De Santo C, Marigo I, Colombo MP, et al. Tumors induce a subset of inflammatory monocytes with immunosuppressive activity on CD8+ T cells. J Clin Invest. 2006; 116:2777–2790. [PubMed: 17016559]
42. Chow EK-H, Fan L-l, Chen X, Bishop JM. Oncogene-specific formation of chemoresistant murine hepatic cancer stem cells. Hepatology. 2012; 56:1331–1341. [PubMed: 22505225]
43. Woodard LE, Keravala A, Jung WE, Wapinski OL, Yang Q, Felsher DW, et al. Impact of hydrodynamic injection and phiC31 integrase on tumor latency in a mouse model of MYC-induced hepatocellular carcinoma. PLoS One. 2010; 5:e11367. [PubMed: 20614008]
44. Liu F, Song Y, Liu D. Hydrodynamics-based transfection in animals by systemic administration of plasmid DNA. Gene Ther. 1999; 6:1258–1266. [PubMed: 10455434]
45. Evan GI, Wyllie AH, Gilbert CS, Littlewood TD, Land H, Brooks M, et al. Induction of apoptosis in fibroblasts by c-myc protein. Cell. 1992; 69:119–128. [PubMed: 1555236]

46. Borrello MG, Alberti L, Fischer A, Degl'innocenti D, Ferrario C, Gariboldi M, et al. Induction of a proinflammatory program in normal human thyrocytes by the RET/PTC1 oncogene. Proc Natl Acad Sci U S A. 2005; 102:14825–14830. [PubMed: 16203990]
47. Xu K, Shu HK. EGFR activation results in enhanced cyclooxygenase-2 expression through p38 mitogen-activated protein kinase-dependent activation of the Sp1/Sp3 transcription factors in human gliomas. Cancer Res. 2007; 67:6121–6129. [PubMed: 17616668]
48. Yang L, Karin M. Roles of tumor suppressors in regulating tumor-associated inflammation. Cell Death Differ. 2014; 21:1677–1686. [PubMed: 25190145]
49. Di Mitri D, Toso A, Chen JJ, Sarti M, Pinton S, Jost TR, et al. Tumour-infiltrating Gr-1+ myeloid cells antagonize senescence in cancer. Nature. 2014; 515:134–137. [PubMed: 25156255]
50. Kennedy Alyssa L, Morton Jennifer P, Manoharan I, Nelson David M, Jamieson Nigel B, Pawlikowski Jeff S, et al. Activation of the PIK3CA/AKT Pathway Suppresses Senescence Induced by an Activated RAS Oncogene to Promote Tumorigenesis. Molecular Cell. 2011; 42:36–49. [PubMed: 21474066]
51. Browning JD, Horton JD. Molecular mediators of hepatic steatosis and liver injury. J Clin Invest. 2004; 114:147–152. [PubMed: 15254578]
52. Gabrilovich DI, Ostrand-Rosenberg S, Bronte V. Coordinated regulation of myeloid cells by tumours. Nat Rev Immunol. 2012; 12:253–268. [PubMed: 22437938]
53. Ruffell B, Affara NI, Coussens LM. Differential macrophage programming in the tumor microenvironment. Trends Immunol. 2012; 33:119–126. [PubMed: 22277903]
54. Grivennikov SI, Greten FR, Karin M. Immunity, Inflammation, and Cancer. Cell. 2010; 140:883–899. [PubMed: 20303878]
55. Murdoch C, Muthana M, Coffelt SB, Lewis CE. The role of myeloid cells in the promotion of tumour angiogenesis. Nat Rev Cancer. 2008; 8:618–631. [PubMed: 18633355]
56. Sun B, Karin M. Inflammation and liver tumorigenesis. Front Med. 2013; 7:242–254. [PubMed: 23681888]
57. Fang CH, Zhang GQ, Zhu XY, Gong JQ. Distribution of oval cells and c-myc mRNA expression in mouse hepatocarcinogenesis. Hepatobiliary Pancreat Dis Int. 2004; 3:433–439. [PubMed: 15313684]

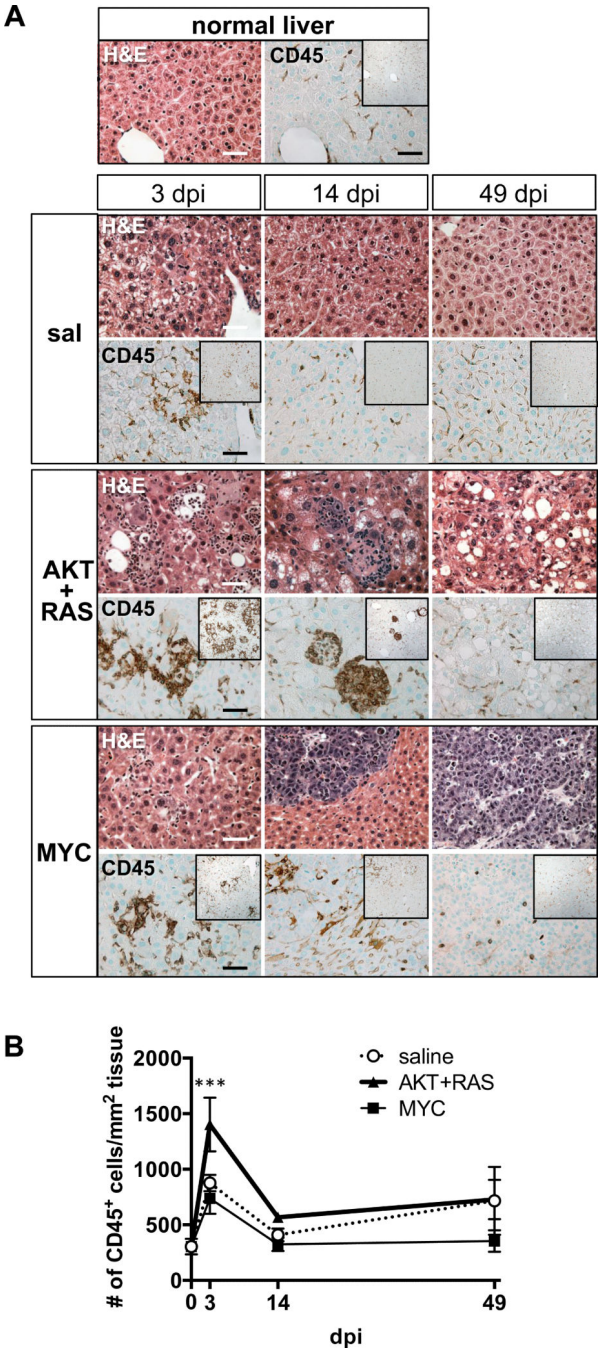

Fig. 1. Inflammation during *MYC*- and *AKT/RAS*-driven liver tumorigenesis

H&E and CD45 staining (brown) in perfused livers of mice hydrodynamically injected with saline, or with Sleeping Beauty transposon system carrying *AKT/RAS* or *MYC*. Scale bar=50 μm. **(B)** Quantification of CD45 immunostaining. Zero time point represents untreated livers. Data are displayed as mean ± SEM with n=3 mice per group. Significance (*AKT/RAS* 3 dpi *vs* normal liver) was determined by two-way ANOVA and Tukey's multiple comparisons post-hoc test (***p<0.001).

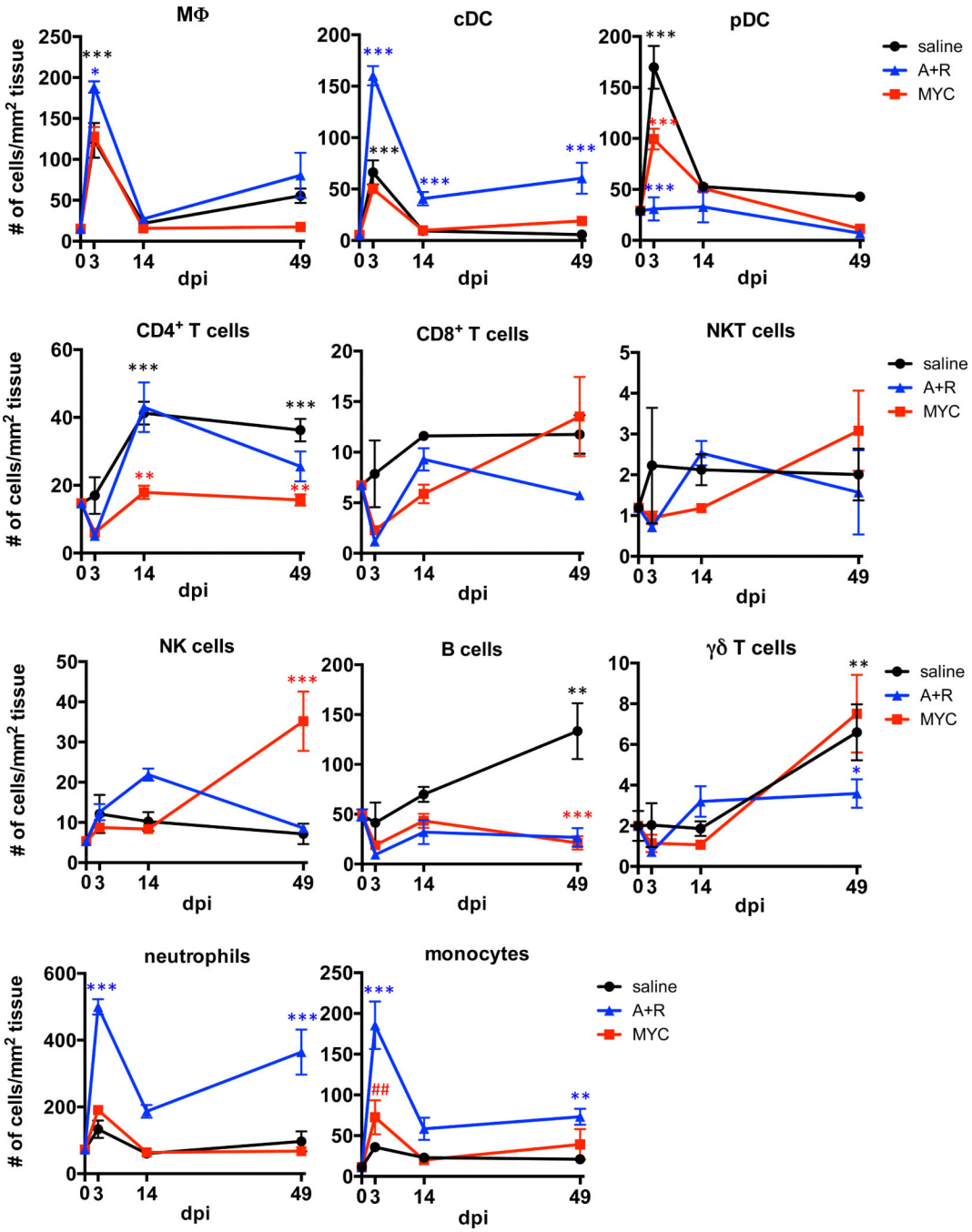

Fig. 2. Distinct profiles of liver-infiltrating leukocytes during *MYC*- and *AKT/RAS*-driven tumorigenesis

Immunophenotyping based on the expression of multiple lineage markers detected by flow cytometry. Oncogene-treatments were compared to time-matched saline controls (red asterisks for *MYC*, blue for *AKT/RAS*). Saline controls were compared to untreated (zero time point) samples to assess the effect of hydrodynamic transfection alone (black asterisks). Monocyte abundance in *MYC*-transfected livers compared to untreated ($^{\#\#}p<0.01$). Data are displayed as mean ± SEM with n=3 mice per group. Significance was determined by two-way ANOVA and Tukey's post-hoc test (*p<0.05, **p<0.01, ***p<0.001).

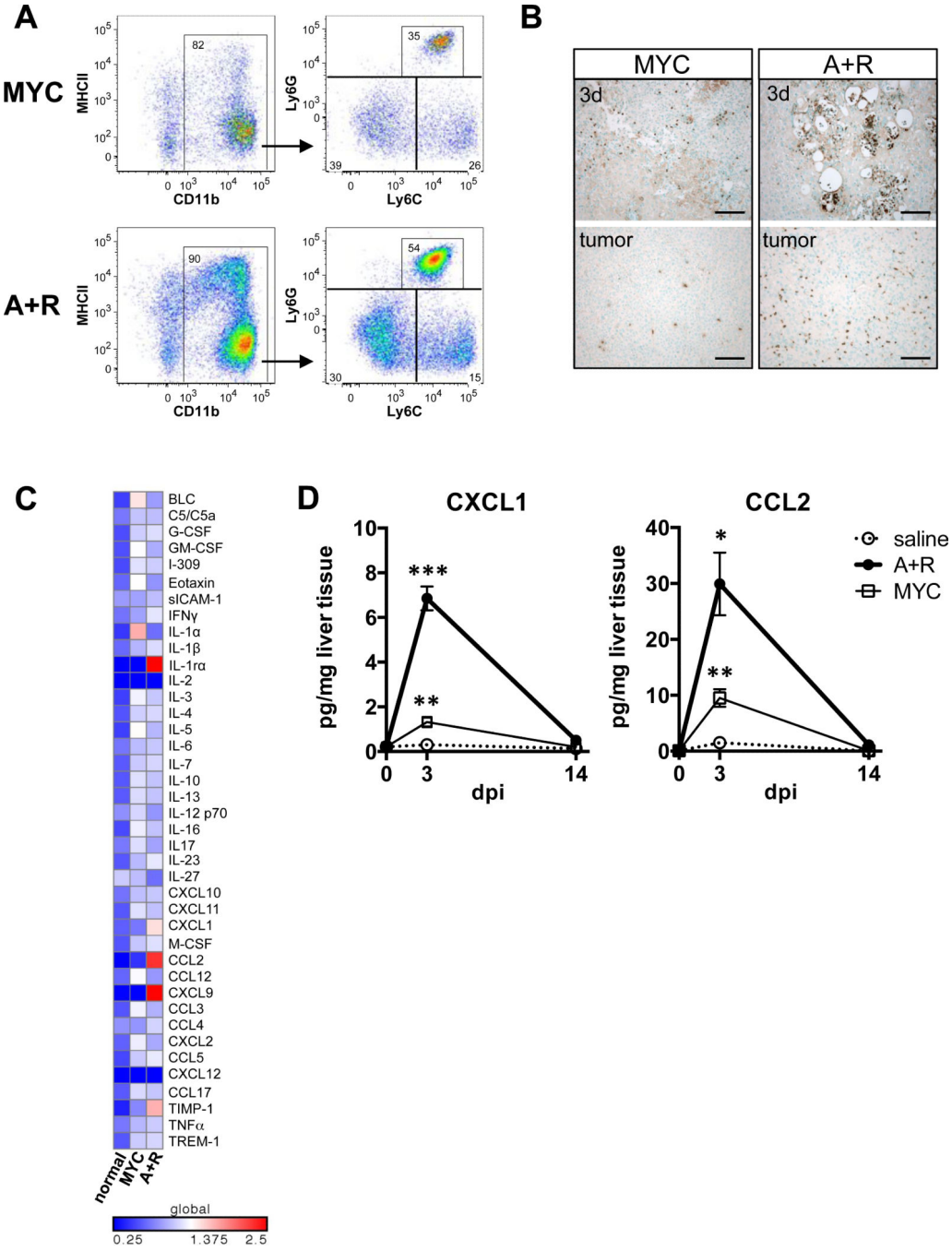

Fig. 3. Marked Ly6G$^+$ neutrophil and Ly6C$^+$ monocyte infiltration and higher CXCL1 and CCL2 levels in the livers of *AKT/RAS*-transfected mice

(A) Dot plots showing the gating of live/CD45$^+$/CD3CD19CD49$^-$ cells for detection of neutrophils (CD11b$^+$Ly6G$^+$Ly6C^{int}) and monocytes (CD11b$^+$Ly6G$^-$Ly6C^{hi}) in *MYC* and *AKT/RAS* tumors. **(B)** 7/4 antigen immunoreactivity (brown) in the livers of *MYC* and *AKT/RAS* mice at 3 dpi and in tumors (50 dpi). Scale bar=100 μm. **(C)** Heat map representing cytokine/chemokine expression in normal livers and *MYC* and *AKT/RAS* liver tumors, measured by protein array (n=1 sample per condition). **(D)** Quantitative ELISA

measurements of CXCL1 and CCL2 in the livers of saline-injected, and *AKT/RAS*- or *MYC*-transfected mice. Data are displayed as mean ± SEM with n≥4 mice/group. Statistical significance was calculated using unpaired t-test.

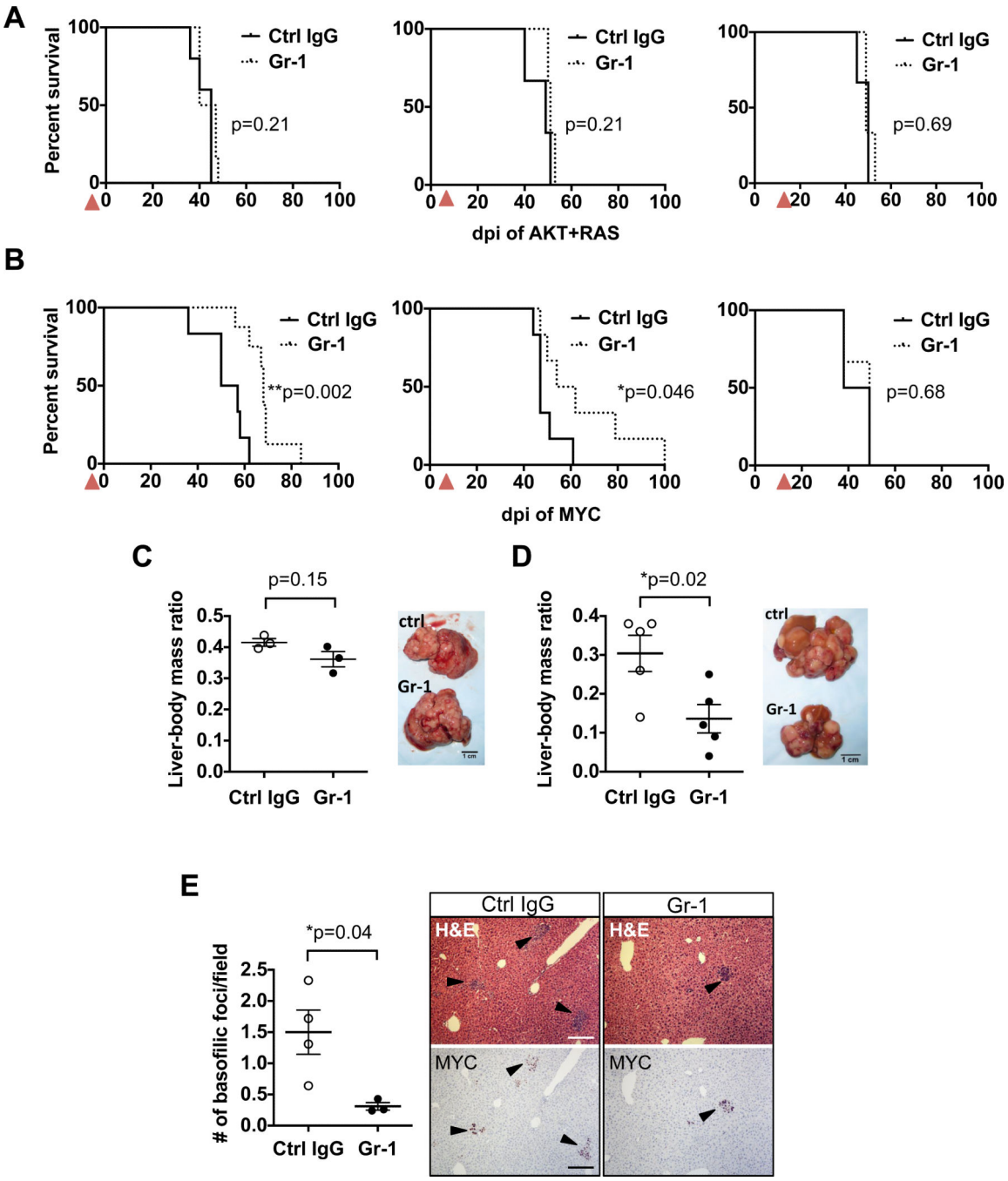

Fig. 4. Gr-1$^+$ leukocytes augment *MYC*- but not *AKT/RAS*-driven tumorigenesis

Survival of *AKT/RAS* **(A)** or *MYC* **(B)** mice treated with anti-Gr-1. Red triangles mark anti-Gr-1 treatments starting at −1, +4, or +16 dpi (log-rank test **p<0.01, *p<0.05; n≥3 mice/group). *AKT/RAS* **(C)** and *MYC* **(D)** tumor burden at 5 weeks. Anti-Gr-1 mAb treatment began at −1 dpi (*p<0.05, n≥3 mice/group). **(E)** Quantification of basophilic foci (arrows) in *MYC*-transfected livers at 7 dpi (*p<0.05, n=3). Representative H&E and MYC immunostaining are shown. Scale bar=200 μm. Data **(C-E)** are displayed as mean ± SEM with n≥3 mice/group. Statistical significance was calculated using unpaired t-test.

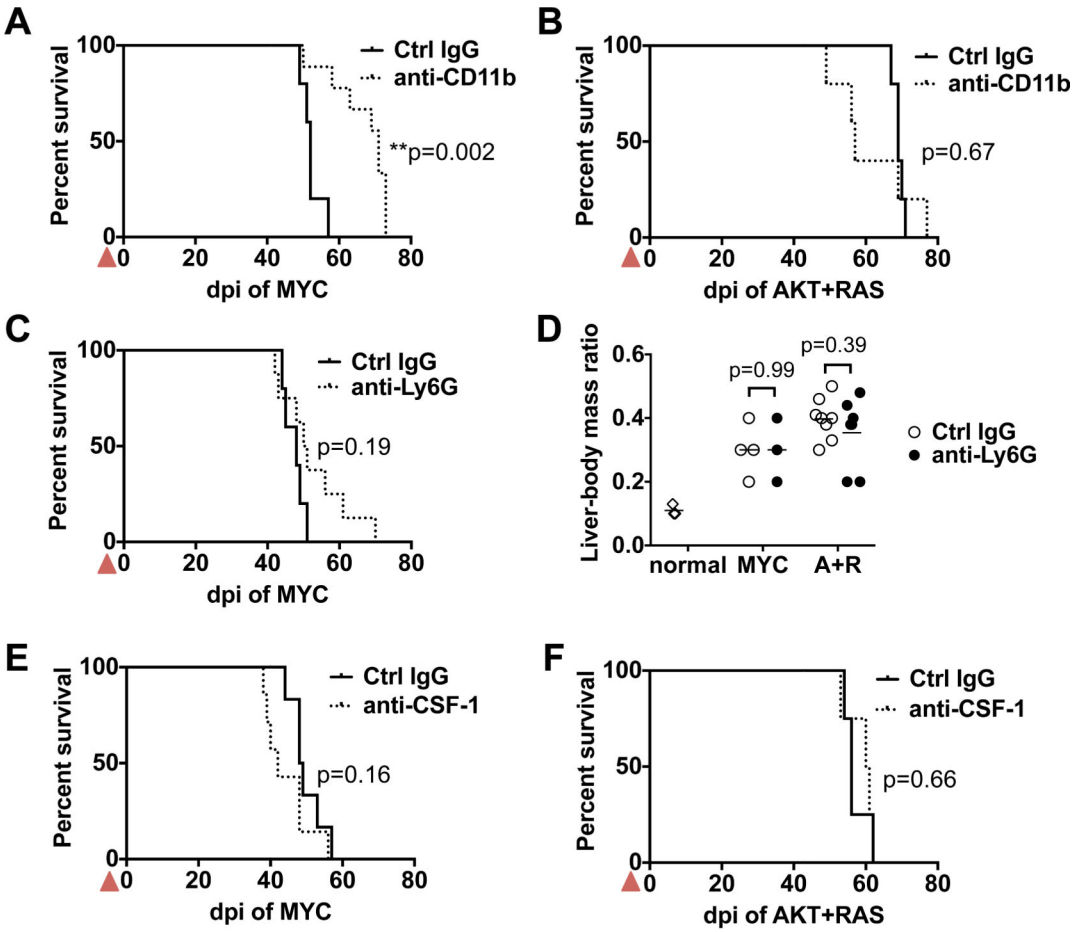

G

Antibody:	Gr-1 (Ly6C/G)	1A8 (Ly6G)	CD11b	CSF-1
Cells targeted:	MO, NE	NE	MO/MΦ, NE	MΦ
Effect on *MYC*-driven tumorigenesis:	Extends survival	No effect	Extends survival	No effect

Fig. 5. Ly6C$^+$ monocytes selectively enhance *MYC*-driven tumorigenesis

Survival of anti-CD11b-treated *MYC* **(A)** or *AKT/RAS* **(B)** mice (log-rank **p<0.01; n≥5 mice/group). **(C)** Survival of anti-Ly6G-treated *MYC* mice (log-rank p=0.19; n≥5 mice/group). **(D)** Effect of anti-Ly6G on *MYC* (p=0.99) or *AKT/RAS* (p=0.27) tumor burden at 7 weeks after transfection. Data represent mean ± SEM with n≥3 mice/group. Statistical significance was calculated using unpaired t-test. Survival of anti-CSF-1-treated *MYC* **(E)** or *AKT/RAS* **(F)** mice (log-rank *MYC* p=0.16, n≥6 mice/group; *AKT/RAS* p=0.66, n≥4 mice/group). All antibody treatments started one day before oncogene transfection (red triangles). **(G)** Effect of depletional antibodies on *MYC*-driven tumorigenesis (MO-monocytes, NE-neutrophils, MΦ-macrophages).

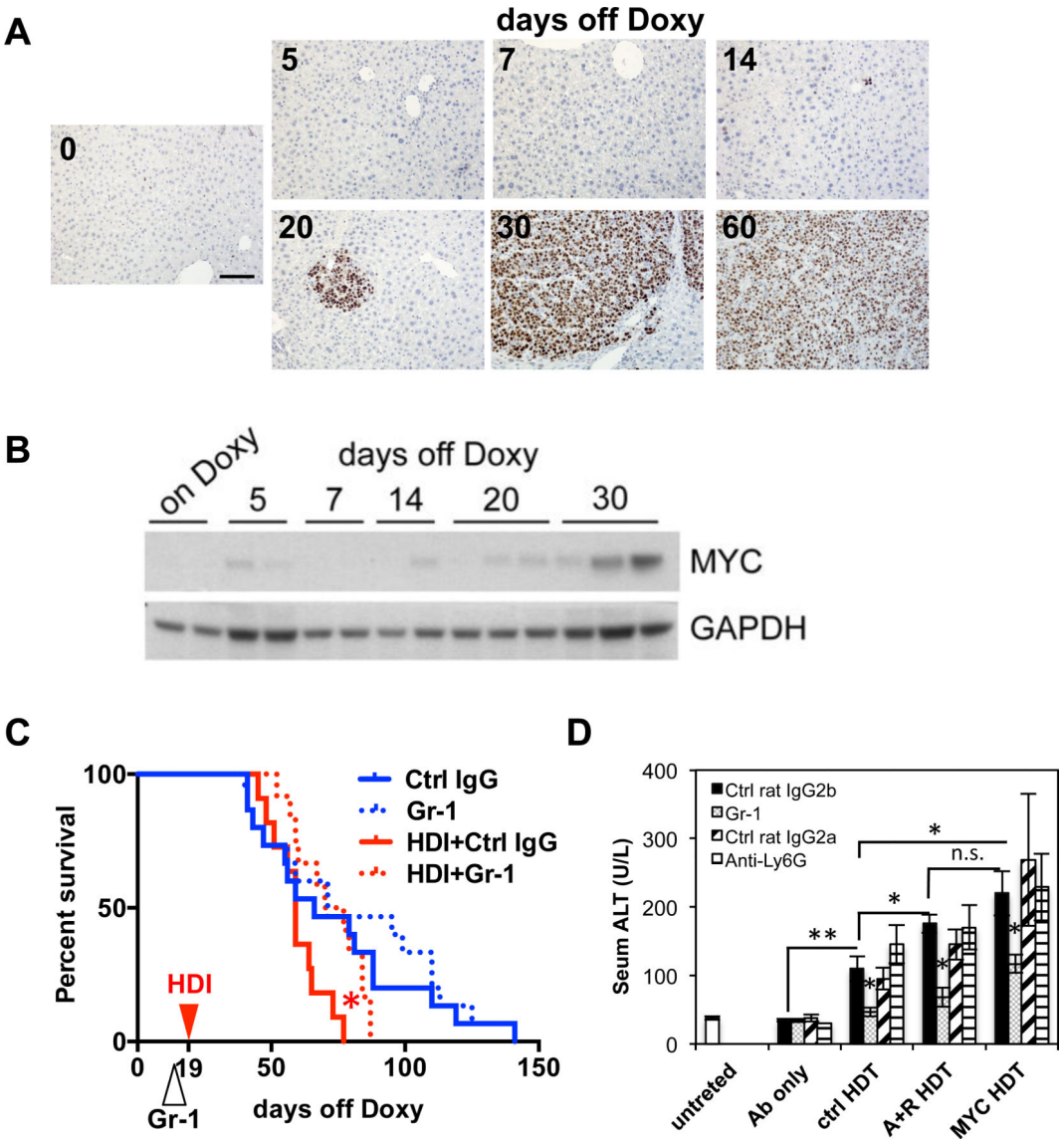

Fig. 6. Gr-1^{+} monocyte-dependent liver injury augments *MYC*-driven tumorigenesis

(A) MYC immunoreactivity in LT2-MYC livers after doxycycline removal (days off Doxy). Scale bar=100 μm **(B)** Immunoblot detection of MYC and GAPDH in LT2-MYC liver lysates. **(C)** Survival of anti-Gr-1-treated, uninjured LT2-MYC mice (blue lines; log-rank p=0.6, n≥8 mice/group) and LT2-MYC mice hydrodynamically injected with saline (HDI) (red lines; log-rank *p=0.01, n≥11 mice/group). Ctrl IgG-treated LT2-MYC mice (Ctrl IgG) *versus* saline-injected LT2-MYC mice (HDI+Ctrl IgG) log-rank p=0.07. **(D)** Effect of anti-Gr-1 and anti-Ly6G treatment (started at -1 dpi) on serum ALT levels 3 days after control hydrodynamic transfection (ctrl HDT) or transfection of *AKT/RAS* (A+R HDT) or *MYC* (MYC HDT). Data represents mean ± SEM with n≥3 mice/group. Significance was determined using unpaired t-test (*p<0.05, **p<0.01).